

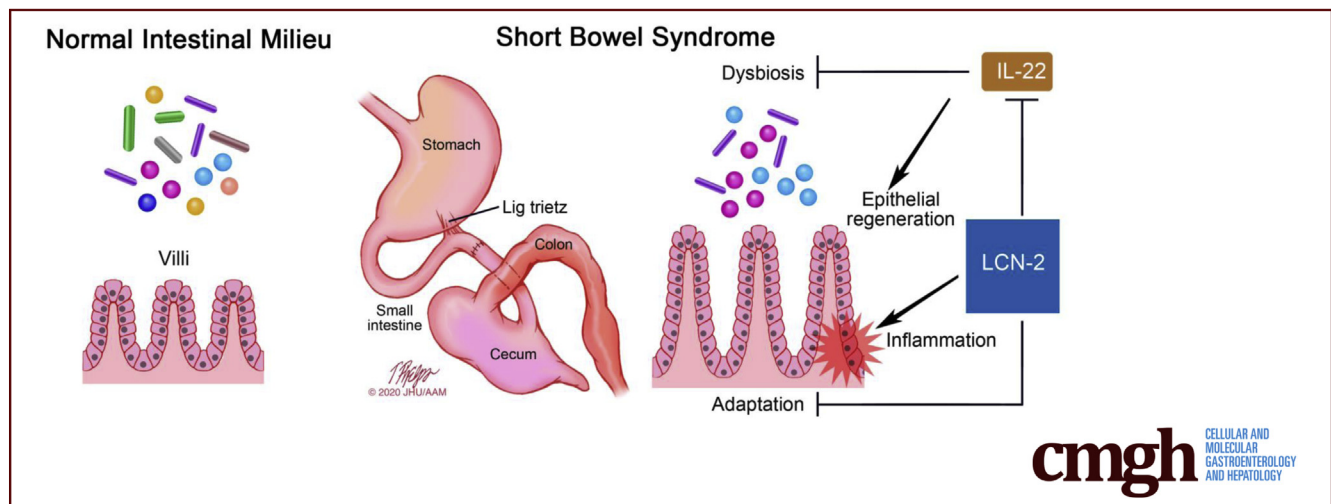
ORIGINAL RESEARCH

A Central Role for Lipocalin-2 in the Adaptation to Short-Bowel Syndrome Through Down-Regulation of IL22 in Mice



Ailan Zhang,¹ Chhinder P. Sodhi,¹ Menghan Wang,¹ Darla R. Shores,² William Fulton,¹ Thomas Prindle,¹ Serena Brosten,¹ Elizabeth O'Hare,¹ Alexander Lau,¹ Hua Ding,² Hongpeng Jia,¹ Peng Lu,¹ James R. White,³ Justin Hui,⁵ Cynthia L. Sears,⁴ David J. Hackam,¹ and Samuel M. Alaish¹

¹Department of Surgery, ²Department of Pediatrics, ⁴Department of Medicine, ⁵Department of Biomedical Engineering, Johns Hopkins University School of Medicine, Baltimore, Maryland; ³Resphera Biosciences, Baltimore, Maryland



SUMMARY

Compared with wild-type mice, lipocalin-2^{-/-} mice have increased interleukin 22 expression, increased adaptation, and less dysbiosis after 75% small-bowel resection. Moreover, the proinflammatory and anti-adaptive effects of lipocalin-2 can be transferred to germ-free mice via a fecal transplant.

BACKGROUND & AIMS: In short-bowel syndrome (SBS), inadequate intestinal adaptation is responsible for the majority of complications, including sepsis, liver failure, and death. In this study, we sought to further delineate the adaptive response to identify potential therapeutic targets.

METHODS: We performed a 75% small-bowel resection (SBR) or sham operation on C57Bl/6J wild-type (WT), lipocalin-2 (LCN2)^{-/-}, and interleukin 22 (IL22)^{-/-} mice. Exogenous IL22 was administered to SBR WT mice. Cecal fecal matter from SBR WT and SBR LCN2^{-/-} mice were transplanted into germ-free mice. Intestinal permeability, inflammation, proliferation, and the microbiome were evaluated 1 week after surgery. CD4⁺IL22⁺ lamina propria lymphocytes were sorted by flow

cytometry. Naïve T cells were polarized to T-helper cells with or without LCN2.

RESULTS: A 75% SBR in a mouse re-creates the increased intestinal permeability, enterocyte proliferation, and intestinal dysbiosis seen in SBS. LCN2 expression increases after 75% SBR, and this increase can be abrogated with broad-spectrum antibiotic treatment. LCN2^{-/-} mice have less intestinal inflammation, increased IL22 expression, and greater adaptation as evidenced by less intestinal permeability, increased carbohydrate enzyme expression, less weight loss, and less dysbiosis after 75% SBR than WT mice. The proinflammatory and anti-adaptive effects of LCN2 can be transferred to germ-free mice via a fecal transplant. Administration of exogenous IL22 improves adaptation and restores the normal microbiome after 75% SBR in WT mice.

CONCLUSIONS: LCN2 promotes inflammation and slows intestinal adaptation through changes in the microbiome and IL22 inhibition in a mouse SBS model. Strategies to reduce LCN2 may offer novel therapeutic approaches to enhance adaptation in SBS. (*Cell Mol Gastroenterol Hepatol* 2020;10:309–326; <https://doi.org/10.1016/j.jcmgh.2020.04.006>)

Keywords: Microbiome; Fecal Transplant; Dysbiosis; Small-Bowel Resection.

The malabsorptive wstate known as short-bowel syndrome (SBS) has devastating consequences. Most SBS patients are infants, who typically develop SBS after an extensive bowel resection for either a congenital anomaly or a postnatal condition, such as necrotizing enterocolitis.^{1,2} SBS patients develop intestinal failure and require prolonged parenteral nutrition.¹⁻³ Complications of SBS include cholestasis,¹⁻³ increased intestinal permeability,¹ and an intestinal dysbiosis with a decrease in bacterial diversity and an increase in Proteobacteria, which produce lipopolysaccharide and are proinflammatory in nature.⁴⁻⁶ Intestinal permeability increases with this intestinal dysbiosis,⁷ and these recurrent infections are known to increase liver dysfunction⁸ and reduce bile flow into the intestine, which weakens the intestinal barrier.^{9,10} Current clinical management of SBS patients to derail this vicious cycle is limited to prophylactic antibiotics^{1,2} to combat the dysbiosis and decrease infections; however, this therapy has low efficacy with many adverse effects, including the emergence of resistant bacteria and fungal overgrowth, culminating in formidable infections. A better understanding of the mechanisms involved in intestinal barrier homeostasis during this period of adaptation is vital to augmenting the adaptive response through new focused molecular therapies.

Changes in the intestinal microbiota have been shown to lead to changes in intestinal resistance,⁷ showing the interplay between the two. Recently, Marchix et al¹¹ noted that the microbiota is a key mediator of gut homeostasis and a potential driver of metabolism and immunomodulation after intestinal loss. Lipocalin-2 (LCN2) is a glycoprotein expressed in neutrophils and intestinal epithelial cells that is involved in the antibacterial innate immune response.¹² LCN2 binds to siderophores, which are bacterial peptides that bind iron, and thus prevents bacterial iron uptake and acts as a bacteriostatic agent.^{13,14} Moreover, LCN2^{-/-} mice have been shown to have decreased survival after Proteobacteria (*Escherichia coli*) infection compared with wild-type (WT) control mice.¹⁵ Our laboratory previously showed that the LCN2 gene and messenger RNA (mRNA) expression increases after cholestasis in a cholestatic mouse model,¹⁶ and Wildhaber et al¹⁷ showed up-regulation of *Lcn2* gene expression in mice that underwent a 70% small-bowel resection (SBR) 1 week earlier; however, a link between LCN2 and SBS remained to be established. These findings led us to hypothesize that LCN2 expression increases after SBS and leads to changes in the microbiota and improved intestinal adaptation. To test this hypothesis, we chose the 75% SBR mouse model originally described by Helmraath et al¹⁸ because it re-creates the malabsorption seen in SBS and retains the powerful advantage of easy genetic manipulations to study mechanisms involved in the host-gut microbiota crosstalk in intestinal adaptation. Hence, we were able to study the contribution of LCN2 and interleukin (IL)22 by subjecting LCN2^{-/-} and IL22^{-/-} mice, respectively, to this model.


We now show that LCN2 expression increased after SBS; however, contrary to our hypothesis, this increased LCN2 expression led to increased inflammation and a detrimental effect on intestinal adaptation through a mechanism that was associated with an increased intestinal dysbiosis and IL22 inhibition. Furthermore, rescue therapy with exogenous IL22 improved adaptation and counteracted the dysbiosis seen in our SBS model. These findings support LCN2 inhibition and IL22 potentiation as potential therapeutic targets to augment intestinal adaptation in SBS.

Results

75% SBR in a Mouse Re-creates Increased Intestinal Permeability, Enterocyte Proliferation, and Intestinal Dysbiosis Seen in SBS

Consistent with a massive SBR, mice entering the current model of SBS lost 10%–15% of their body weight by 7 days, whereas the sham-operated mice started to gain weight after 1 day and recovered quickly to baseline by postoperative day (POD) 7 (Figure 1A). Importantly, the SBS mice had markedly increased enterocyte proliferation as evidenced by increased bromodeoxyuridine staining in the intestinal crypts and along the villi (Figure 1B), increased intestinal permeability noted by increased serum fluorescence after fluorescein isothiocyanate (FITC)-dextran gavage feeding (Figure 1C), and increased villi length showing adaptation (Figure 1D–F); all of these findings are seen in SBS patients¹ and lend validity to the current model. DNA analysis of the cecal contents of the SBS and sham-operated mice on POD 7 clearly show different bacterial populations, as shown via the β -diversity plot (Figure 2A), as well as a trend toward decreased α -diversity in the SBS mice similar to what is seen in SBS patients⁴⁻⁶ (Figure 2B–D). By POD 21, there was significantly less α -diversity in the SBR WT mice as compared with the sham (SHA) WT mice. The SBS mice also had strikingly increased relative abundance of both *Enterococcus*, *Clostridia*, and Proteobacteria, with decreased Bacteroidetes and Firmicutes, which similarly was true in the SBS patient population,⁴⁻⁶ thus further validating our model (Figure 2E–I). These changes in the microbiota prompted us to evaluate the antibacterial peptide LCN2 in the host response to SBS.

Abbreviations used in this paper: ABX, antibiotics; ELISA, enzyme-linked immunosorbent assay; FBS, fetal bovine serum; FITC, fluorescein isothiocyanate; FMT, fecal microbiota transplant; GF, germ-free; IL, interleukin; LCN2, lipocalin-2; LPL, lamina propria lymphocyte; mRNA, messenger RNA; OTU, operational taxonomic units; PBS, phosphate-buffered saline; PCR, polymerase chain reaction; POD, postoperative day; rmlCN2, recombinant mouse lipocalin-2; rRNA, ribosomal RNA; SBS, short-bowel syndrome; SHA, sham; SBR, small-bowel resection; Th22, helper T cell 22; WT, wild-type.

 Most current article

© 2020 The Authors. Published by Elsevier Inc. on behalf of the AGA Institute. This is an open access article under the CC BY-NC-ND license (<http://creativecommons.org/licenses/by-nc-nd/4.0/>).

2352-345X

<https://doi.org/10.1016/j.jcmgh.2020.04.006>

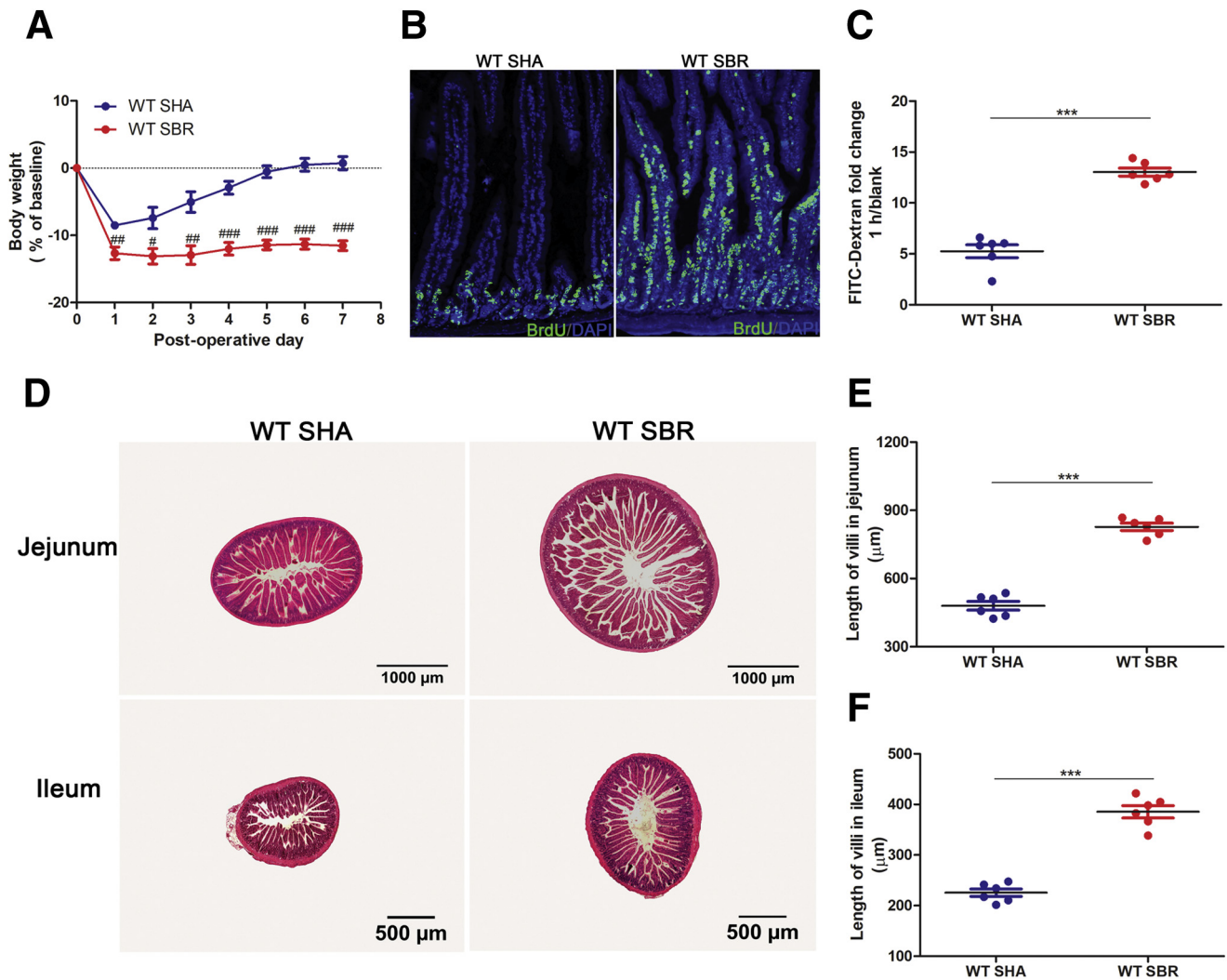


Figure 1. Mice undergoing 75% SBR show significant intestinal adaptation. (A) Body weight changes in SHA ($n = 6$) and 75% SBR ($n = 6$) mice from PODs 1–7. (B) Enterocyte proliferation was assessed by bromodeoxyuridine (BrdU) staining on POD 7. (C) Intestinal permeability was evaluated by the fold change of FITC-dextran in serum on POD 7. (D) Representative H&E-stained sections of jejunum and ileum 7 days after sham or SBR surgery. Scale bars: 1000 μm (jejunum); 500 μm (ileum). (E and F) Length of villi in (E) jejunum and (F) ileum were measured under light microscopy. At least 30 well-oriented intact villi were counted per mouse. Each dot represents a mouse. *** $P < .001$; # $P < .05$, ## $P < .01$, and ### $P < .001$ vs WT SHA. DAPI, 4',6-diamidino-2-phenylindole.

LCN2 Expression in the Intestine and the Liver Increases After 75% SBR

At the onset of our analysis, we found that LCN2 protein secreted into the serum and feces significantly increased after 75% SBR (Figure 3A and B). Further work showed that transcriptional levels of *Lcn2* gene expression in the intestine and liver increased significantly, especially in the jejunum and the liver, after massive SBR, as compared with their sham counterparts (Figure 3C). In concordance, LCN2 protein expression increased significantly ($P < .05$) in both the liver and the intestine, as compared with the sham animals (Figure 3D and E). *Lcn2* mRNA and LCN2 protein expression were higher in the jejunum and ileum than in the colon. Immunofluorescence staining with LCN2 antibody correlated with the Western blot data (Figure 3F) and localized the LCN2-positive cells

to the lamina propria in the villi. Most of the LCN2-positive cells co-localized with the neutrophil marker myeloperoxidase (Figure 3G).

Depletion of Intestinal Microbiota Decreased Intestinal Adaptation in SBS

Combined ampicillin, neomycin, vancomycin, and metronidazole antibiotic (ABX) treatment successfully depleted the intestinal microbiota within 7 days in WT mice, which was evidenced by a significant decrease of the fecal bacterial load (Figure 4C). However, the depletion of intestinal microbiota significantly decreased the survival rate (Figure 4A) and intestinal adaptation in SBR mice with ABX treatment, which lost more body weight (Figure 4B) and had shorter jejunal villi (Figure 4C) compared with SBR

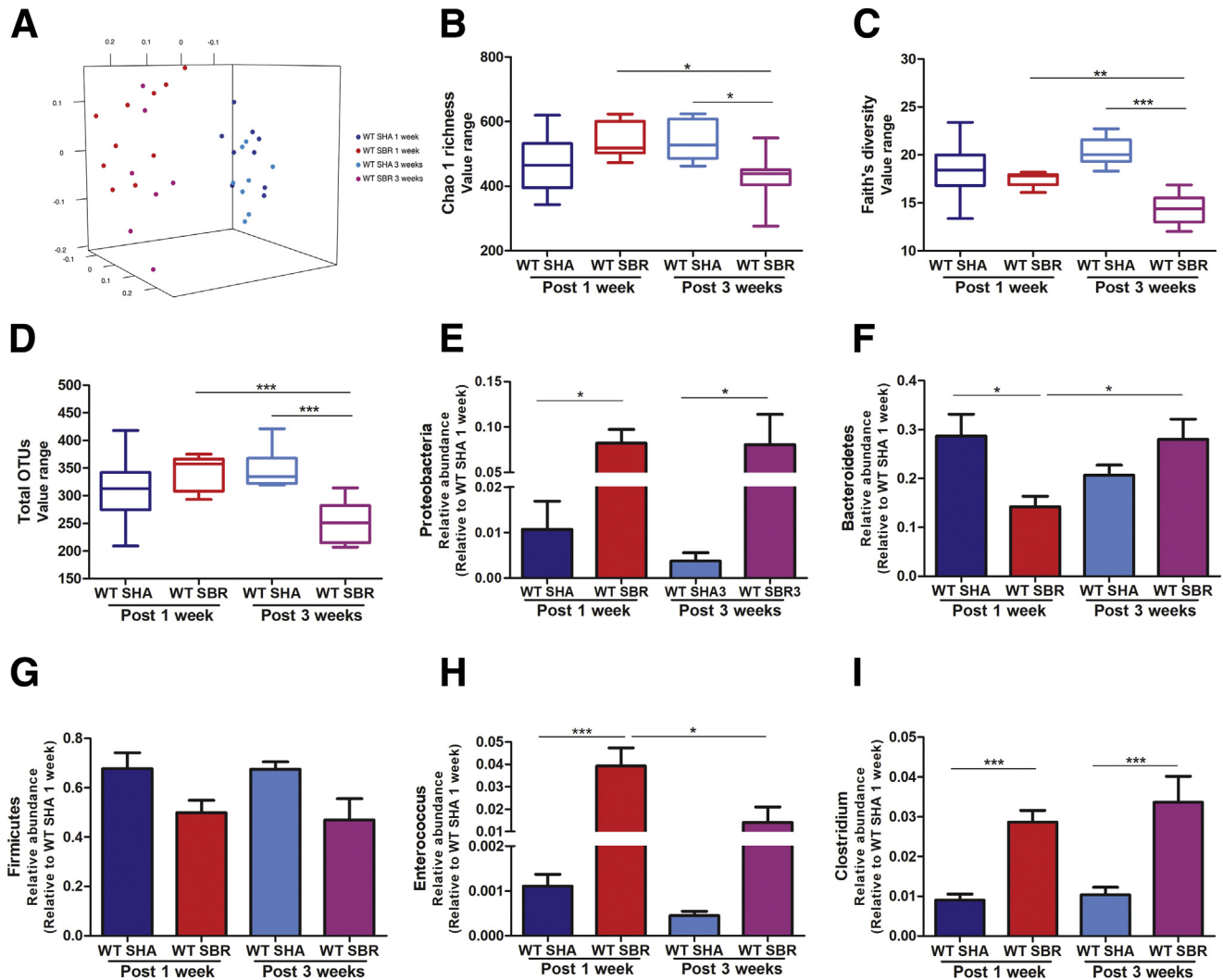


Figure 2. Intestinal dysbiosis occurs in WT mice after 75% SBR. The intestinal microbiome was evaluated by 16S rRNA sequencing on postoperative weeks 1 and 3. (A) β -diversity was shown in a principal component analysis plot: WT SHA after 1 week, n = 9; WT SBR after 1 week, n = 10; WT SHA after 3 weeks, n = 8; WT SBR after 3 weeks, n = 7. Each dot represents a mouse. (B–D) Taxa richness and evenness were evaluated by (B) Chao 1 richness, (C) Faith diversity, and (D) total OTUs. (E–I) Relative abundance of (E) Proteobacteria (F) Bacteroidetes, (G) Firmicutes, (H) *Enterococcus*, and (I) *Clostridium* were assessed in sham and 75% SBR groups. * $P < .05$, ** $P < .01$, and *** $P < .001$.

mice with untreated intestinal microbiota. We also found that ABX treatment abolished LCN2 expression in the intestine and liver (Figure 4E–H), implicating a crosstalk relationship between the microbiome and LCN2 expression. Thus, we concluded that LCN2 plays an important role in the host response to SBS.

LCN2^{-/-} Mice Have Less Intestinal Inflammation and Greater Adaptation as Shown by Less Intestinal Permeability, Increased Carbohydrate Enzyme Expression, Less Weight Loss, Less Dysbiosis, and Greater Survival After 75% SBR Than WT Mice

We hypothesized that LCN2 was beneficial to the host response to SBS and that the absence of LCN2 would be

detrimental. To test our hypothesis, we subjected LCN2^{-/-} mice to our SBR model. Contrary to our hypothesis, we noted that the SBR LCN2^{-/-} mice lost significantly more weight than shams ($P < .05$), but less than SBR WT mice (Figure 5A). Intestinal permeability was increased in SBR LCN2^{-/-} mice as compared with shams ($P < .05$), but significantly less than in SBR WT mice (Figure 5B). The length of the villi in the jejunum and ileum increased significantly after SBR in both WT and LCN2^{-/-} mice (Figure 5C–E). Moreover, the intestinal expression of the carbohydrate enzyme sucrase-isomaltase, and the hepatic expression of the bile acid receptor *Tgr5*, were increased significantly in the SBR LCN2^{-/-} mice as compared with their SBR WT littermates ($P < .05$) (Figure 5F and G). LCN2^{-/-} SBR mice had less regional and systemic inflammation than WT SBR mice, as shown by significantly lower transcriptional

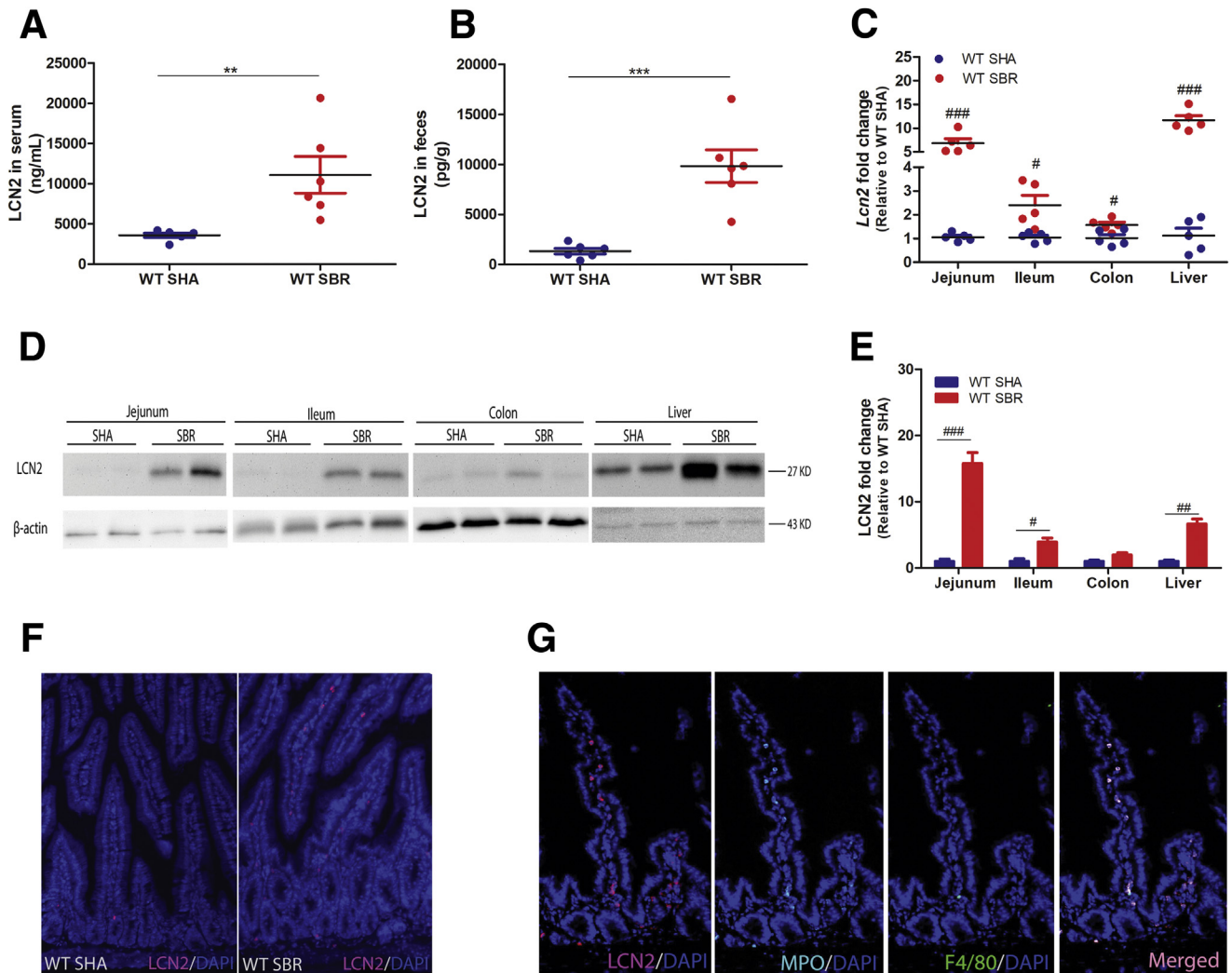


Figure 3. LCN2 expression significantly increases in WT mice after 75% SBR on postoperative day 7. (A and B) LCN2 expression in the (A) serum and (B) feces was measured by ELISA ($n = 6$ mice per group). (C) Transcription levels of the *Lcn2* gene in the intestine and liver were evaluated by quantitative PCR ($n = 5$ per group). (D and E) Representative LCN2 protein expression in the intestine and liver were measured with Western blot analysis ($n = 4$ per group). (F) Representative LCN2-stained sections of jejunum after sham or SBR surgery ($n = 3$ per group). (G) Representative LCN2, myeloperoxidase, and F4/80 co-stained sections of jejunum after SBR surgery ($n = 3$). Each dot represents a mouse. ** $P < .01$ and *** $P < .001$; # $P < .05$, ## $P < .01$, and ### $P < .001$ vs WT SHA. DAPI, 4',6-diamidino-2-phenylindole; MPO, myeloperoxidase.

levels of *Il6* and *Tnf- α* genes in the intestine, and lower IL6 expression levels in the serum (Figure 5H–J).

Chao 1 richness (Figure 6A), Faith diversity (Figure 6B), and total operational taxonomic units (OTUs) (Figure 6C) showed that the taxa richness and evenness were significantly different between WT and *LCN2*^{-/-} mice. There was a significant decrease in the α -diversities of the *LCN2*^{-/-} mice as compared with the WT mice before and after 75% SBR at POD 7. The principal component analysis results showed that the intestinal microbiome profile was clearly divided into 4 groups (Figure 6D). *LCN2*^{-/-} SBR mice had significantly less proinflammatory Proteobacteria (Figure 6E), more Bacteroidetes (Figure 6F), and more Firmicutes (Figure 6G) than WT SBR mice. Indeed, *LCN2*^{-/-} SBR mice were more similar to sham-operated WT mice. We also observed significant loss of Kyoto

Encyclopedia of Genes and Genomes (KEGG) pathways at level 3 for the gut microbiome associated with primary and secondary bile acid biosynthesis in WT mice after 75% SBR, but not in *LCN2*^{-/-} SBR mice (Figure 6H and I). These data indicate that the presence of LCN2 reduces intestinal function during adaptation and leads to a more profound dysbiosis.

The Proinflammatory and Anti-Adaptive Effects of LCN2 Can Be Transferred to Germ-Free Mice via a Fecal Transplant

To define the role of the microbiome in our SBS model, we assessed fecal transplants into germ-free (GF) mice. Stool slurries (4%) from WT SBR and *LCN2*^{-/-} SBR mice were transplanted into GF mice. GF mice

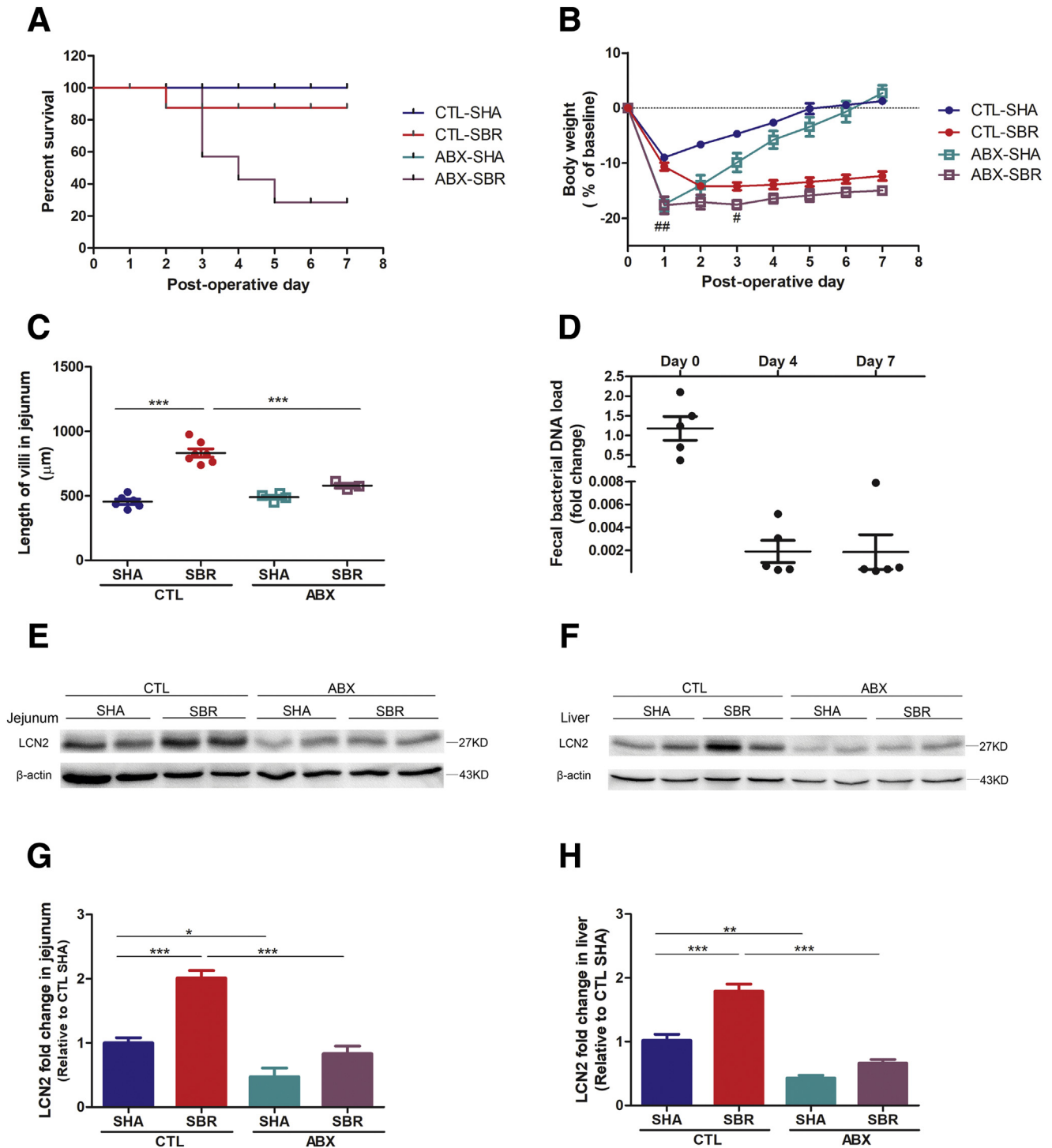
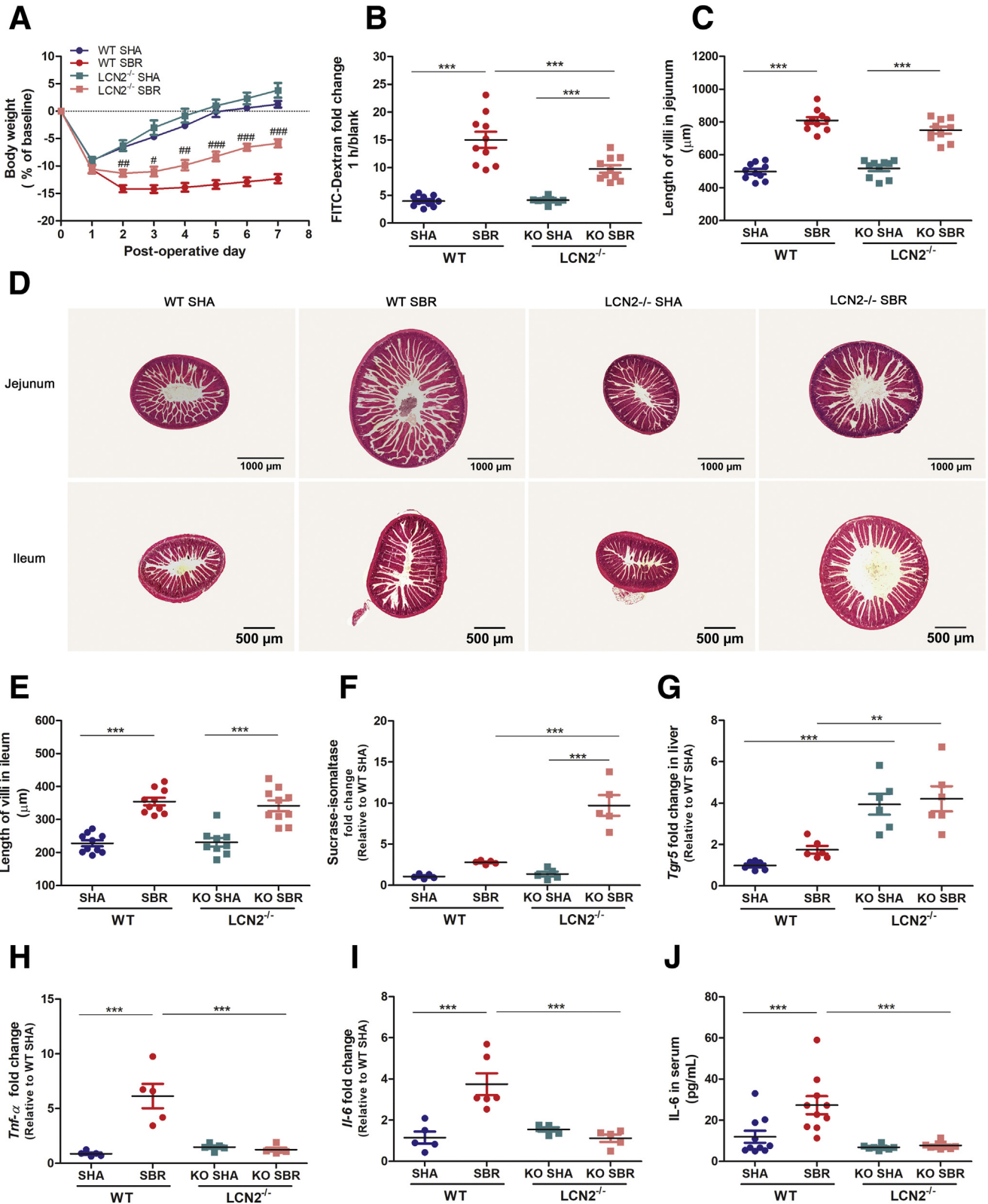


Figure 4. Depletion of intestinal microbiota decreases intestinal adaptation in SBS. (A) Survival rate was evaluated from PODs 1–7, CTL SHA (n = 6), CTL SBR (n = 8), ABX SHA (n = 6), and ABX SBR (n = 8). (B) Body weight changes in CTL SHA (n = 6), CTL SBR (n = 7), ABX-SHA (n = 6), and ABX-SBR (n = 3) from PODs 1–7. (C) Length of villi in jejunum were measured under light microscopy. At least 30 well-oriented intact villi were counted per mouse. (D) Fecal bacterial load was evaluated by quantitative PCR with universal 16S primers. (E–H) LCN2 expression in (E and G) jejunum and (F and H) liver after antibiotic treatment were measured by Western blot analysis. Each dot represents a mouse. * $P < .05$, ** $P < .01$, and *** $P < .001$; # $P < .05$ and ## $P < .01$. CTL, control.

transplanted with SBR WT cecal contents lost 3% of their body weight over 7 days, whereas GF mice transplanted with SBR LCN2^{-/-} cecal contents actually

gained 6% of their body weight (Figure 7A). Consistent with the weight loss seen in the WT SBR transplants, intestinal permeability was higher in GF mice

transplanted with WT SBR fecal matter as compared with those transplanted with SBR LCN2^{-/-} fecal matter (Figure 7B). In addition, the jejunal villi were significantly longer in GF mice transplanted with SBR LCN2^{-/-} fecal matter as compared with those transplanted with SBR WT fecal matter (Figure 7C and D).



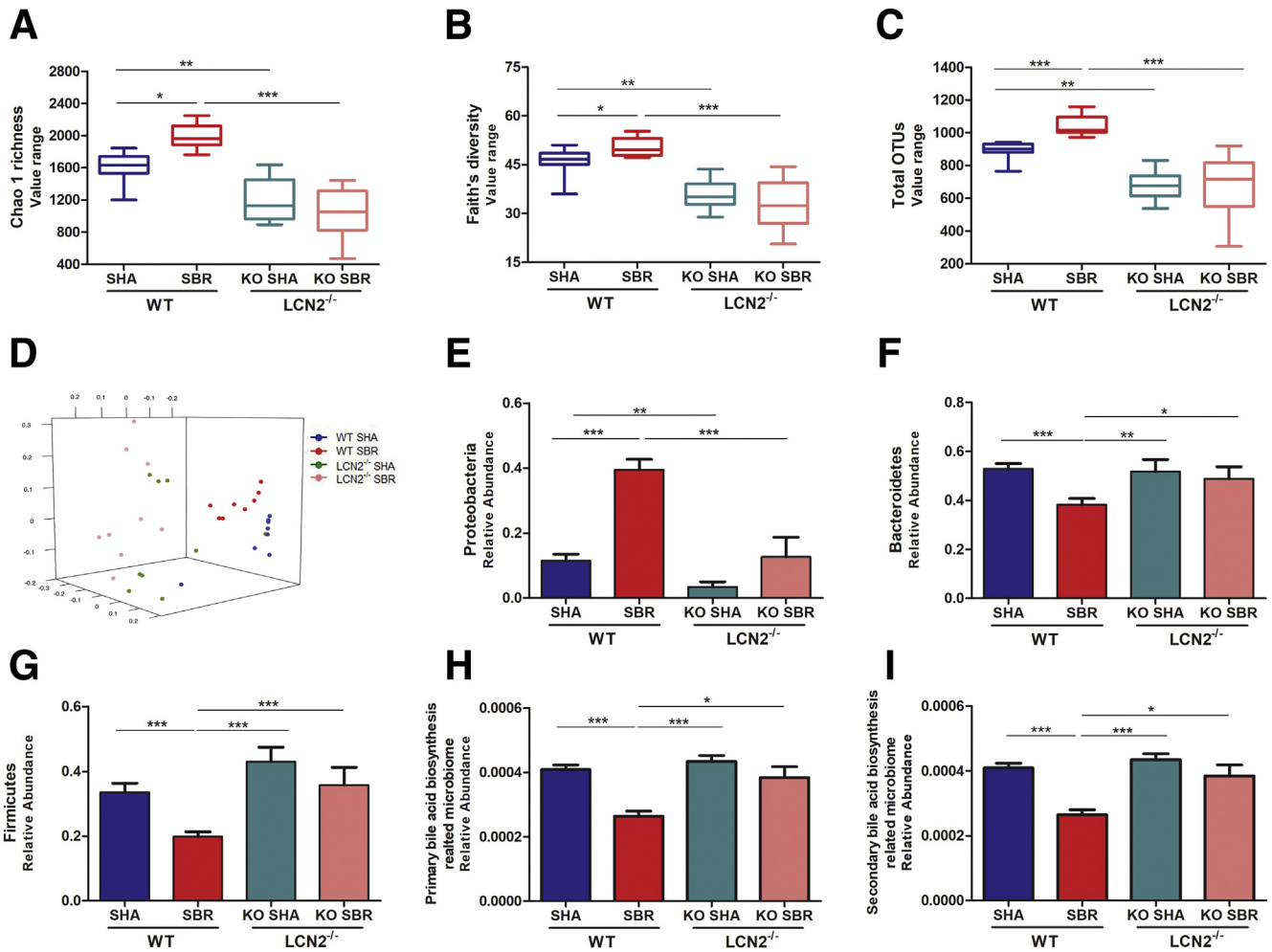


Figure 6. Intestinal microbiome changes in WT and LCN2^{-/-} mice after sham or 75% SBR. The intestinal microbiome was evaluated by 16S rRNA sequencing on POD 7. (A–C) Taxa richness and evenness were evaluated by (A) Chao 1 richness, (B) Faith diversity, and (C) total OTUs. (D) β -diversity is shown in a principal component analysis plot (each dot represents a mouse). (E–G) Relative abundance of (E) Proteobacteria (F) Bacteroidetes, and (G) Firmicutes. WT SHA, n = 8; WT SBR, n = 8; LCN2^{-/-} SHA, n = 8; and LCN2^{-/-} SBR, n = 9. (H and I) Kyoto Encyclopedia of Genes and Genomes (KEGG) pathways at level 3 for the gut microbiome associated with (H) primary and (I) secondary bile acid biosynthesis. * $P < .05$, ** $P < .01$, and *** $P < .001$.

IL22 Augments Intestinal Adaptation After SBR

IL22 is known to be involved in intestinal barrier homeostasis, and IL22^{-/-} mice are known to have compromised intestinal barrier function as compared with WT mice.¹⁹ We hypothesized that the absence of IL22 would be detrimental to intestinal adaptation after SBS. To test this hypothesis, we subjected IL22^{-/-} mice to

our 75% SBR model. Indeed, we found that SBR IL22^{-/-} mice lost more weight than SBR WT mice (Figure 8A). Of note, sham-operated IL22^{-/-} mice had increased intestinal permeability similar to SBR WT mice (Figure 8B). Furthermore, jejunal villi length was decreased in SBR IL22^{-/-} mice as compared with SBR WT mice (Figure 8C–E).

Figure 5. (See previous page). LCN2^{-/-} mice had less intestinal inflammation and greater functional adaptation after 75% SBR than WT mice. (A) Body weight changes in WT and LCN2^{-/-} mice after sham surgery and 75% SBR from PODs 1–7 (n = 10 mice per group). (B) Intestinal permeability was evaluated by the fold-change of FITC-dextran in serum on POD 7 (n = 10 per group). (C and E) The length of the villi in the (C) jejunum and (E) ileum were measured under light microscopy (n = 10 per group). At least 30 well-oriented intact villi were counted per mouse. (D) Representative H&E-stained sections of jejunum and ileum 7 days after sham or SBR surgery. Scale bars: 1000 μ m (jejunum); 500 μ m (ileum). (F) Sucrase-isomaltase (n = 5 per group) and (G) *Tgr5* (n = 6 per group) were quantified by quantitative PCR. (H and I) Transcription levels of (H) *Tnf- α* and (I) *Il6* genes in small intestine were evaluated by quantitative PCR (n = 6 per group). (J) A systemic feature of inflammation, IL6 in serum, was measured by ELISA (n = 10 per group). Each dot represents a mouse. ** $P < .01$ and *** $P < .001$; # $P < .05$, ## $P < .01$, ### $P < .001$ vs WT SBR.

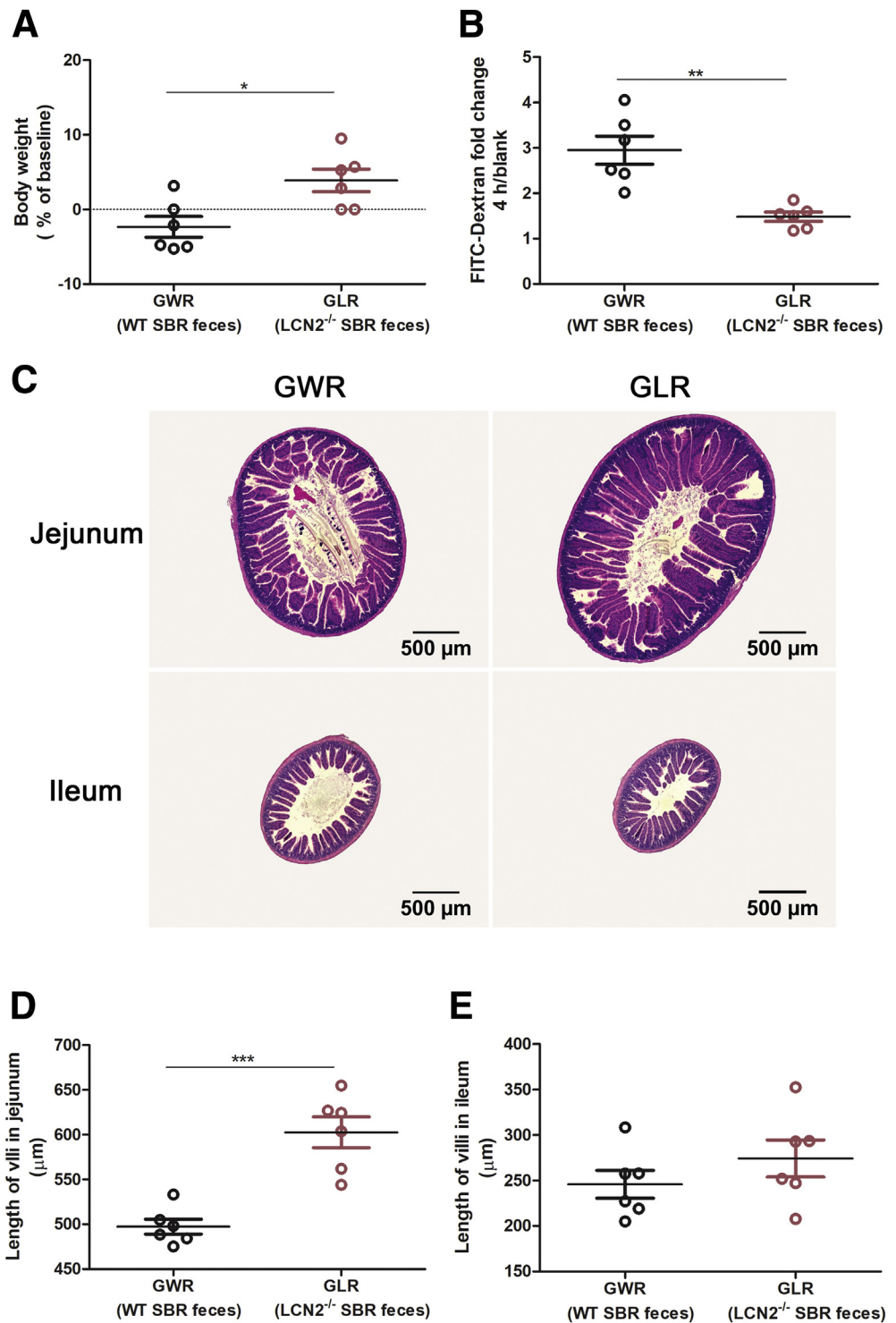


Figure 7. Intestinal adaptation in GF mice after fecal microbiota transplantation. The 4% fecal slurries were created from cecal contents of conventional WT SBR and LCN2^{-/-} SBR mice, and gavage-fed (100 μ L/mouse) to GF mice ($n = 6$ mice per group). (A) Body weight changes in GF mice transplanted with fecal contents from WT SBR or LCN2^{-/-} SBR mice on post-transplant day 7. (B) Intestinal permeability was evaluated by the fold change of FITC-dextran in the serum on post-transplant day 7. (C) Representative H&E-stained sections of the jejunum and the ileum 7 days after fecal microbiota transplantation. Scale bar: 500 μ m. The length of the villi in the (D) jejunum and (E) ileum were measured under light microscopy. At least 30 well-oriented intact villi were counted per GF mouse. GWR ($n=6$), germ-free mice received fecal matters from WT SBR donor; GLR ($n=6$), germ-free mice received fecal matters from LCN2^{-/-} SBR donor. Each dot represents a mouse. * $P < .05$, ** $P < .01$, and *** $P < .001$.

LCN2 Reduces Intestinal Adaptation by Inhibiting IL22 Expression After 75% SBR

Understanding the significance of IL22 in SBS, we examined this cytokine in our SBR WT and SBR LCN2^{-/-} mice. We found that the serum levels of IL22 decreased in SBR WT mice compared with sham-operated controls, whereas serum IL22 did not change in SBR LCN2^{-/-} mice

(Figure 9A). From these data, we hypothesized that LCN2 may inhibit IL22 expression in SBS and reduce adaptation. In vivo transcriptional levels of *Il22* gene expression in the small intestine decreased significantly in SBR WT mice as compared with SHA WT mice, whereas the expression increased significantly in SBR LCN2^{-/-} mice as compared with SHA LCN2^{-/-} mice (Figure 9B). Subsequent isolation of

laminal propria lymphocytes (LPLs) from the small intestine then were analyzed by flow cytometry. The percentage of CD4⁺IL22⁺ cells among LPLs decreased significantly after SBR in WT mice while the percentage of these cells

increased in SBR LCN2^{-/-} mice (Figure 9C). In vitro, we successfully polarized naïve T cells to helper T (Th)22 cells, as shown by a significant increase of IL22 in the supernatant (Figure 9D). Subsequent treatment with exogenous LCN2

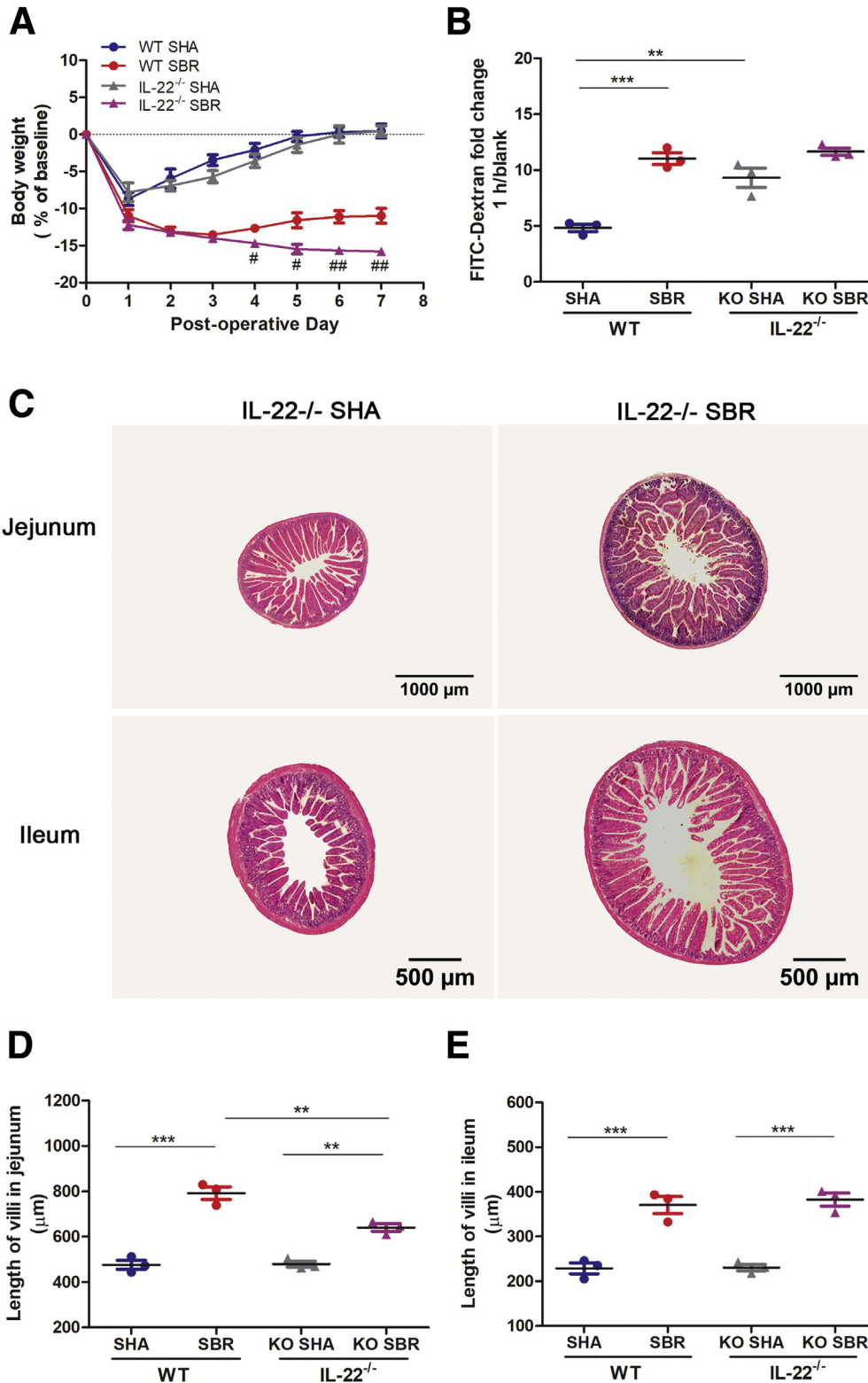


Figure 8. IL22^{-/-} mice had worse intestinal adaptation with less weight gain and shorter jejunal villi after 75% SBR than WT mice. (A) Body weight changes in WT and IL22^{-/-} mice after sham surgery and 75% SBR from PODs 1–7 (n = 3 mice per group). (B) Intestinal permeability was evaluated by the fold-change of FITC-dextran in the serum on POD 7 (n = 3 per group). (C) Representative H&E-stained sections of the jejunum and the ileum 7 days after sham or SBR surgery. Scale bars: 1000 μm (jejunum); 500 μm (ileum). (D and E) The length of villi in the (D) jejunum and the (E) ileum were measured under light microscopy (n = 3 per group). At least 30 well-oriented intact villi were counted per mouse. Each dot represents a mouse. **P < .01 and ***P < .001; #P < .05 and ##P < .01.

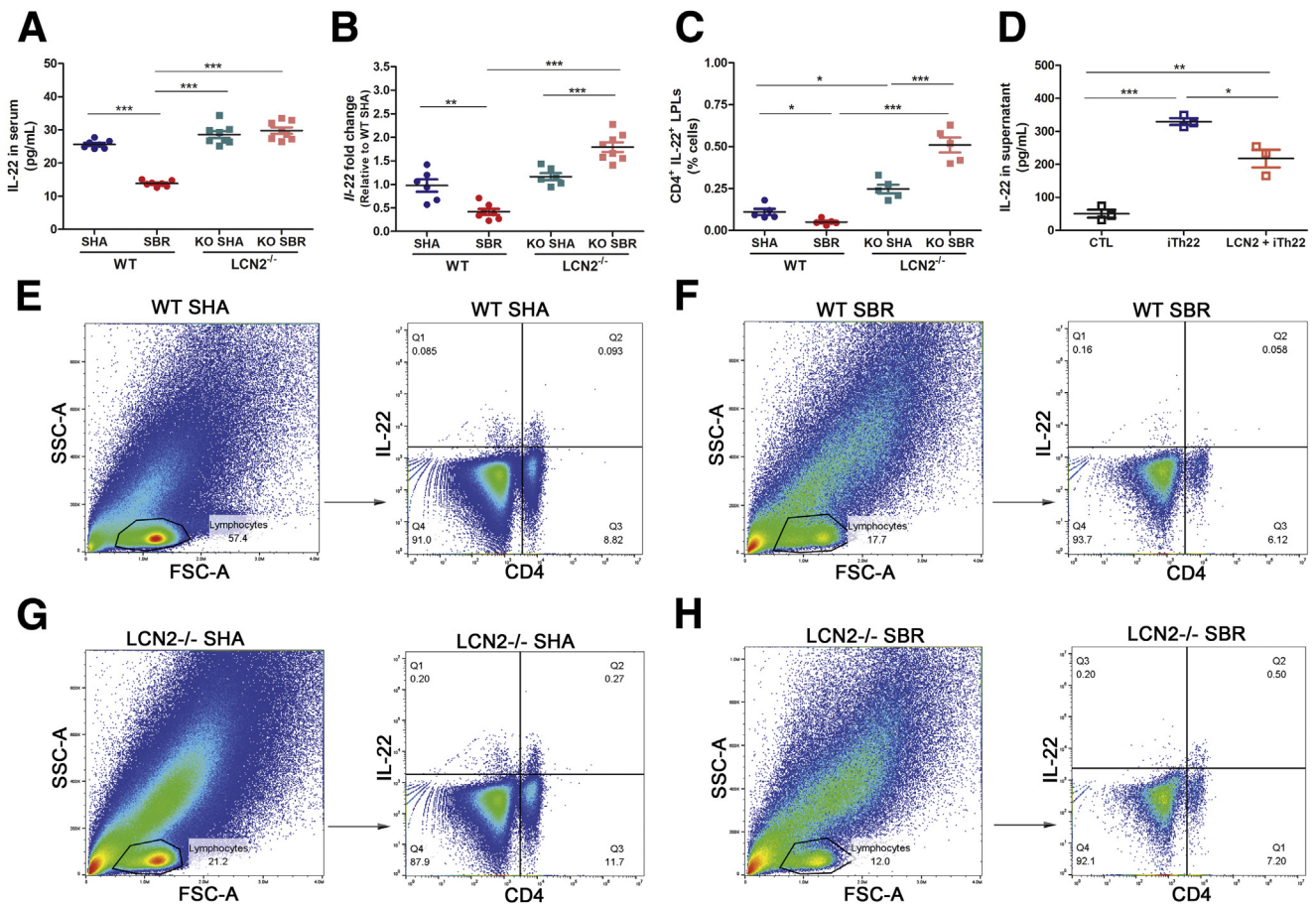


Figure 9. LCN2 reduces intestinal adaptation by inhibiting IL22 expression after 75% SBR on POD 7. (A) IL22 protein expression in the serum was measured by ELISA ($n = 7$ mice per group). (B) Transcriptional levels of the *Il22* gene in the intestine were evaluated by quantitative PCR ($n = 6$ per group). (C) $CD4^+IL22^+$ LPLs were quantified with flow cytometry analysis ($n = 5$ per group). (D) Representative IL22 protein expression in supernatant from Th22 cells in vitro with and without LCN2 stimulation as measured by ELISA ($n = 3$ per group/each experiment, each experiment was repeated 3 times). (E–H) Representative flow cytometry dot plots of the LPL population from small intestinal tissue. Single-cell suspensions prepared from the lamina propria were stained with CD4 and IL22 antibodies. Gate 1 identified lymphocytes based on FSC-A/SSC-A properties. The numbers within the quadrants represent the percentage of $CD4^+IL22^-$, $CD4^+IL22^+$, $CD4^-IL22^-$, and $CD4^-IL22^+$ cells within the lymphocyte gate. Data are representative of analyses of 5 mice per group. Forward scatter area (FSC-A)/side scatter area (SSC-A). * $P < .05$, ** $P < .01$, and *** $P < .001$.

decreased the levels of IL22 protein expression significantly (Figure 9D). Taken together, these data outline a mechanism through which LCN2 reduces intestinal function during adaptation after SBS by inhibiting *IL22* gene expression.

IL22 Improves Intestinal Adaptation and Counteracts Dysbiosis After 75% SBR

To determine if restoration of IL22 could rescue the SBR WT mice from impaired adaptation and dysbiosis, we treated SBR WT mice with either phosphate-buffered saline (PBS) or recombinant mouse (rm)IL22 via intraperitoneal injections. On POD 7, PBS-treated SBR WT mice had lost 11% of their body weight, whereas the rmIL22-treated SBR WT mice had only lost 7.5% of their body weight (Figure 10A). Compared with the PBS-treated group, the rmIL22-treated mice had significantly longer jejunal villi (Figure 10B), although there was no difference in the length of ileal villi between these 2 groups (Figure 10C). We also

assessed the transcription levels of the IL22-mediated antibacterial peptide genes *Reg3b* and *Reg3g* in both the jejunum and colon. The rmIL22 treatment triggered a robust increase of both *Reg3b* and *Reg3g* in both the jejunum and the colon (Figure 10D–G). However, IL22 induced inflammation with increased transcriptional levels of *Tnf- α* in the jejunum (Figure 10H). Importantly, rmIL22 treatment counteracted the intestinal dysbiosis in SBS as evidenced by decreased relative amounts of proinflammatory Proteobacteria (Figure 10I) and increased relative amounts of healthy Bacteroidetes (Figure 10J) and Firmicutes (Figure 10J) in the cecal contents. These data support IL22 as a therapeutic target to augment intestinal adaptation in SBS.

Discussion

In agreement with our earlier observation that LCN2 mRNA expression increased after common bile duct ligation¹⁶

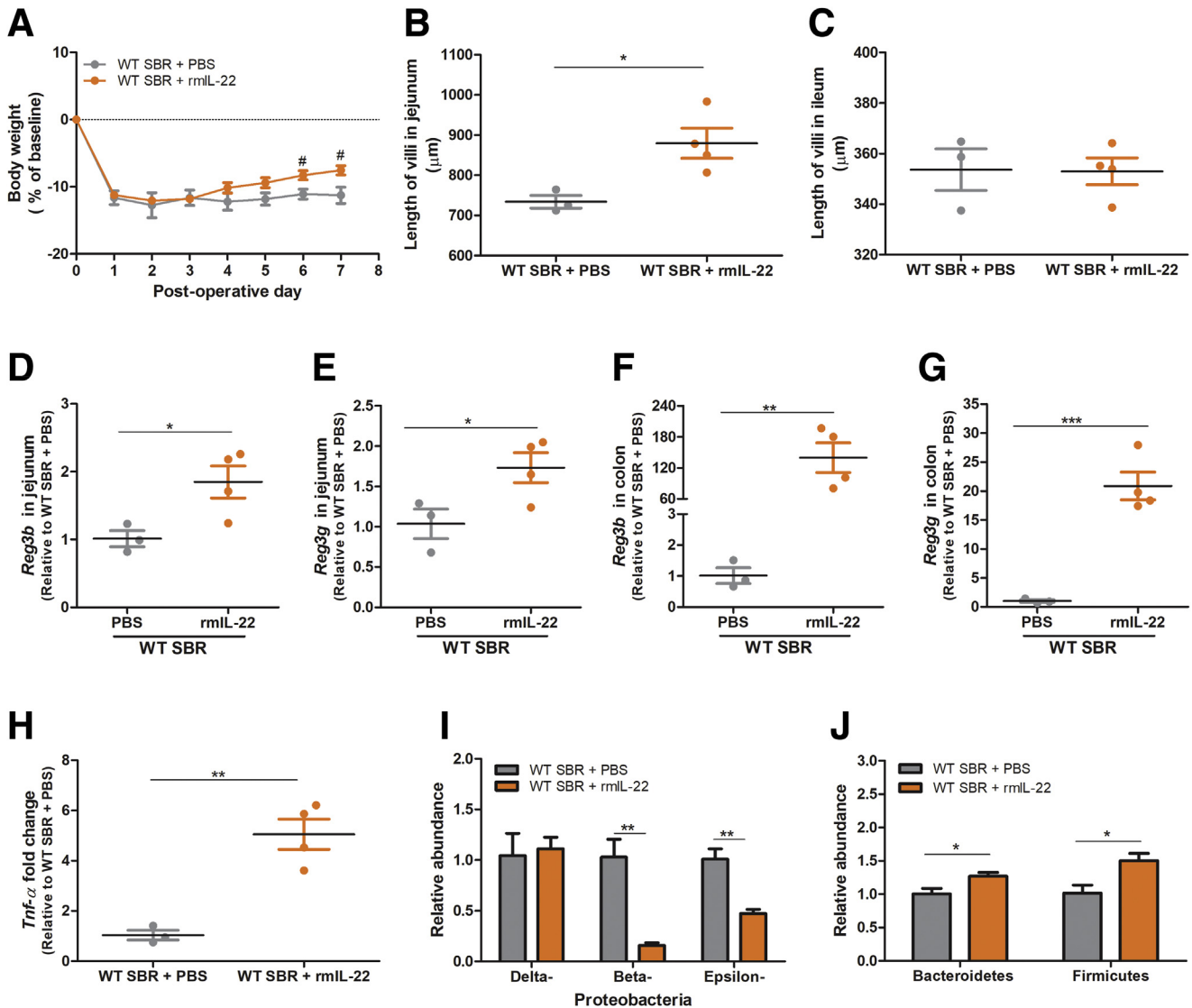


Figure 10. IL22 promotes intestinal adaptation and counteracts the dysbiosis seen after 75% SBR. (A) Body weight changes in WT mice treated with either PBS ($n = 3$ mice) or rmlL22 ($n = 4$) after 75% SBR from PODs 1–7. (B and C) The length of villi in the (B) jejunum and the (C) ileum were measured under light microscopy. At least 30 well-oriented intact villi were counted per mouse. (D and E) Transcriptional levels of IL22-mediated antibacterial peptides (D) *Reg3b* and (E) *Reg3g* in the jejunum. (F and G) Transcriptional levels of (F) *Reg3b* and (G) *Reg3g* in the colon. (H) Transcriptional levels of *Trif- α* in the jejunum were measured by quantitative PCR. (I and J) Relative abundance of (I) Proteobacteria and (J) Bacteroidetes and Firmicutes were evaluated by quantitative PCR. Each dot represents a mouse. * $P < .05$, ** $P < .01$, and *** $P < .001$; and # $P < .05$.

and the finding by Wildhaber et al of increased LCN2 gene expression after 70% SBR in a mouse,¹⁷ we found that both LCN2 mRNA and protein expression increased in our 75% SBR mouse model. We had hypothesized that this was reflective of a host defense mechanism given LCN2's role as a bacteriostatic agent, however, we found the opposite. Increased LCN2 expression had a detrimental effect on intestinal adaptation and survival. Given the role of LCN2 in other proinflammatory conditions, this is not entirely surprising. LCN2 has been shown to play an active role in nonalcoholic steatohepatitis,²⁰ cardiovascular disease,^{21,22} and obesity/metabolic syndrome.²³ In fact, serum LCN2 has been reported as a marker for the severity of disease in inflammatory bowel disease

patients.²⁴ We found LCN2^{-/-} mice that underwent SBR to have decreased jejunal levels of the proinflammatory cytokines IL6 and TNF- α , and evidence of increased intestinal adaptation with improved weight gain, increased jejunal villi length, increased carbohydrate enzyme expression, and increased survival as compared with WT SBR mice. One possible explanation is that the inflammatory nature of LCN2 supersedes its bacteriostatic effects. Interestingly, we found that antibiotic treatment of SBR WT mice had decreased LCN2 expression, thus highlighting the interplay between the intestine and the microbiome; however, these antibiotic-treated mice also gained less weight, had poorer adaptation, and decreased survival compared with vehicle-treated SBR WT

mice, showing adverse effects from the antibiotics. This result correlates with our general understanding that antibiotics cause less bacterial diversity and a less healthy gut. Consequently, a more focused therapy on LCN2 or its mechanism is required.

To better understand the predominant role of LCN2 in SBS, we investigated the microbiome of these SBR mice. Similar to SBS patients, we found that WT SBR mice had a relative increase in the abundance of proinflammatory bacteria, such as Proteobacteria, as well as Enterococcus, with a decrease in healthy bacteria such as Firmicutes. SBR LCN2^{-/-} mice had less dysbiosis, with levels of Proteobacteria and Firmicutes similar to sham-operated animals. Enterococcus levels were not significantly different from SBR WT mice. This may be explained by the bacteriostatic effect of LCN2 on gram-negative bacteria. These microbiome changes also resulted in functional changes because primary and secondary bile acid biosynthesis, which were reduced in SBR WT mice, were found to be similar to sham-operated animals in SBR LCN2^{-/-} mice. These beneficial effects on the microbiome coincided with a decrease in the intestinal permeability of these mice, highlighting the interplay between the microbiome and intestinal barrier homeostasis. To showcase this relationship in our model, we performed fecal transplantation. Although fecal microbiota transplantation is best known as the new standard treatment for recurrent *Clostridium difficile* colitis,²⁵ other experimental uses of fecal transplantation that show promise include the treatment of inflammatory bowel disease and obesity/metabolic syndrome.²⁵ In our study, we used this approach with the goal of increasing intestinal adaptation and barrier strength in GF mice. GF mice are valuable experimental tools for showing host-microbe interactions. Moreover, genetically modified GF mice can be used to study interactions between any particular gene and the microbiota.²⁶ We showed that fecal transplantation from SBR LCN2^{-/-} donors decreased intestinal permeability and improved weight gain in GF mice, whereas fecal transplantation from SBR WT mice donors led to increased intestinal permeability and weight loss in GF mice. These findings support the dynamic that exists between the intestinal barrier and the microbiome. Furthermore, it suggests that the microbiome changes after SBR precede the intestinal barrier dynamics to influence intestinal adaptation. The current findings illustrate the host gut-microbiota crosstalk in intestinal adaptation described by Marchix et al.¹¹ Moreover, our data increase our understanding of the pathophysiology associated with SBS by greatly expanding the role for LCN2, which previously was thought to be merely a bacteriostatic agent, to include anti-adaptive properties.

We next sought to determine a mechanism behind this LCN2 effect. We found that serum IL22 decreased significantly in SBR WT, but not in SBR LCN2^{-/-}, mice. IL22 has a dual nature, protective vs inflammatory, in modulating the responses of the tissue during an immune response.²⁷⁻³⁰ IL22 can be anti-inflammatory in acute inflammatory models, such as hepatitis,³¹ as well as during chronic inflammation such as inflammatory bowel disease.^{32,33} On the other hand, IL22 was found to be essential in mediating

inflammation in a mouse model of dermal inflammation.³⁴ IL22 also is important for control of the overgrowth of pathogenic bacteria prone to translocation from the gut lumen through the intestinal barrier into the circulation. Hammer et al.³⁵ found that IL22 administration restored the numbers of proliferating cells within crypts and resulted in complete reduction of overgrowth of Enterobacteriaceae in the small intestine after ethanol and burn injury in a mouse model. Thus, the dual nature of IL22 likely depends on the inflammatory context, which includes the duration and amount of IL22 present, the overall cytokine milieu, and the tissues involved.²⁷ It will be challenging to optimize the treatment dose of IL22, which maximizes the beneficial effects of tissue regeneration and host-defense while minimizing the inflammation-induced injury. Restoration of IL22 by neutralization of LCN2 may be a better option.

IL22 is known to be involved in intestinal barrier homeostasis, and IL22^{-/-} mice are known to have increased intestinal permeability as compared with WT mice.¹⁹ We subjected IL22^{-/-} mice to 75% SBR and found increased weight loss and intestinal permeability as compared with SBR WT mice. Re-examining our SBR LCN2^{-/-} mice, we found increased *IL22* gene expression in the small intestine. More specifically, flow cytometry showed increased expression of CD4⁺IL22⁺ LPLs in the small intestine of SBR LCN2^{-/-} mice compared with SBR WT mice. We hypothesized that LCN2 inhibited IL22. To test this, we isolated naïve T cells from the spleen of WT mice, polarized them to become Th22 cells, and then treated them with rmLCN2. Indeed, we found decreased IL22 synthesis in the cells treated with rmLCN2, thus suggesting this as a mechanism of action for LCN2's detrimental effect on intestinal adaptation. This led us to select IL22 as a therapeutic target in our SBR WT mice. Exogenous IL22 rescue therapy did in fact improve adaptation, as evidenced by weight gain and increased villi length, and counteract the dysbiosis seen in our SBR WT mice by reducing the relative amount of Proteobacteria while increasing the amount of Bacteroidetes.

Our findings add depth to our knowledge of IL22-mediated mechanisms. Previous work has shown that pathologic microbiota, such as Proteobacteria, are crucial to the development of inflammation.³⁶ In our 75% SBR model, the relative abundance of Proteobacteria increased markedly, causing a significant increase in LCN2 expression. A concomitant decrease in IL22 expression then led to inflammation and suboptimal adaptation. Most importantly, the elimination of LCN2 or the addition of IL22 can prevent these changes and improve adaptation.

In summary, we observed an increase in LCN2 expression after 75% SBR in a mouse model of SBS. This increased LCN2 expression was associated with increased inflammation, decreased intestinal adaptation, increased intestinal permeability, and a more profound intestinal dysbiosis after 75% SBR compared with SBR mice who lacked this gene. Moreover, increased LCN2 expression was associated with decreased IL22 expression in both the serum and CD4⁺IL22⁺ LPLs in the small intestine of SBR WT mice, thus suggesting an inhibitory pathway. Decreased IL22 synthesis by Th22 cells treated with rmLCN2 in vitro support this as a

possible mechanism. Further research is needed to confirm this mechanism and identify the principals in the pathway. Nevertheless, inhibition of LCN2 has the potential to be a prime therapeutic target as exemplified in our rescue experiment. This type of mechanism-focused therapy to augment intestinal adaptation and decrease parenteral nutrition dependence and the associated infectious complications in SBS without the use of antibiotics warrants continued investigation. Some SBS patients who fail to progress to enteral autonomy may have exaggerated LCN2 expression with reduced IL22 expression. If clinical studies confirm this suspicion, then these patients would be an ideal study population in the future.

Materials and Methods

Animals

Under the Johns Hopkins University Animal Care and Use Committee–approved protocol MO18M194, we performed a 75% SBR on either C57BL/6J, LCN2^{-/-}, or IL22^{-/-} mice, which mimics the resection seen in some SBS patients. Respective sham-operated C57BL/6J, LCN2^{-/-}, and IL22^{-/-} mice served as controls. C57BL/6J WT and LCN2^{-/-} mice were obtained from Jackson Laboratories (Bar Harbor, ME). IL22^{-/-} mice were obtained from Genentech, Inc (South San Francisco, CA). Conventional mice were bred and housed at Johns Hopkins University Animal Facility with a 12-hour light-dark cycle, and given rodent chow ad libitum after weaning. At 5 weeks of age, male conventional mice were housed individually and fed with rodent liquid diet (Bio-serv, F1259SP; Lieber-DeCarli '82, Flemington, NJ) for 4 days before surgery. A rodent liquid diet was maintained during the postoperative period. Fecal microbiota transplant (FMT) was performed in GF mice (C57BL/6J background), which were bred and housed in the GF mouse core at Johns Hopkins University.

Creation of a Clinically Relevant Model of SBS in the Mouse

In our laboratory, we established the model previously described by Helmuth et al¹⁸. Briefly, the hair on the abdomen of the mouse was removed by depilatory cream and the abdomen was scrubbed with 3 rounds of betadine before making an incision. Through a 1.5-cm midline laparotomy, the small bowel was examined. The 75% SBR was performed by transecting the small intestine 3-cm distal to the ligament of Treitz and 6-cm proximal to the cecum. The intervening proximal small bowel (approximately 18 cm) was removed. Intestinal continuity was restored with a primary end-to-end jejunoileal anastomosis using 8-0 nylon sutures. The sham surgery was performed by transecting the small bowel 6-cm proximal to the cecum and immediately creating a primary end-to-end ileoileal anastomosis. Subcutaneous closure was performed with a running absorbable 4-0 Vicryl suture (Ethicon Inc, Cincinnati, OH). Cutaneous closure was completed with interrupted 4-0 silk sutures. All animals received 1 mL saline subcutaneously immediately after surgery.

After surgery, mice were offered free access to water for the first 24 hours. Fresh rodent diet was provided and body weight was measured daily. Bromodeoxyuridine (00-0103; Invitrogen, Carlsbad, CA) was administered via an intraperitoneal injection 24 hours before euthanasia. Intestinal permeability was evaluated with the FITC-dextran intestinal permeability assay described later. Serum, intestinal tissue, liver, and cecal luminal contents were collected at euthanasia 1 week after surgery.

FITC-Dextran Intestinal Permeability Assay

Mice were fasted for 2 hours. Serum was collected before the FITC-dextran administration as the blank. Then, the mice were gavage-fed FITC-dextran (44 mg/100 g, FD4; Sigma, St. Louis, MO). Serum was collected again 1 hour afterward in conventional mice and 4 hours afterward in GF mice. Fluorescence was measured on samples diluted with PBS (1:2) using an excitation wavelength of 490 nm and an emission wavelength of 520 nm. Fold changes of FITC-dextran in the serum 1 hour/blank or 4 hours/blank were calculated.

Depletion of Murine Intestinal Microbiota

Four-week-old WT C57BL/6J male mice were administered an antibiotic cocktail (vancomycin hydrochloride [0.5 g/L, V-200, USP; Gold Biotechnology, St. Louis, MO], metronidazole [1 g/L, M-840, USP; Gold Biotechnology], neomycin sulfate [1 g/L, N-620, USP; Gold Biotechnology], and ampicillin sodium [1 g/L, A-301, USP; Gold Biotechnology]) in the rodent liquid diet (BioServe F1259SP) for 2 weeks before their SBR. The liquid diet and antibiotic cocktail were made fresh and refilled daily in the feeding tube. The control group was administered rodent liquid diet only. Mouse fecal pellets were collected on days 0, 4, and 7 during antibiotic cocktail treatment. Fecal DNA were isolated with the Dneasy PowerSoil kit (12888-100; Qiagen, Carlsbad, CA) according to the manufacturer's instruction. Microbiota depletion was confirmed by fecal total bacterial load via 16S ribosomal RNA (rRNA) polymerase chain reaction (PCR) assay in both the ABX cocktail treatment group and the control group. 16S rRNA universal primers were as follows: 5'-ACTCCTACGGGAGGCAGCAGT-3' and 5'-ATTACCGCGTCTGCTGGC-3'. Survival rate, body weight, length of villi in the jejunum, and LCN2 protein expression in the jejunum and liver were assessed by Western blot.

Assessment of LCN2, IL6, and IL22

LCN2, IL6, and IL22 in serum and feces were quantified with enzyme-linked immunosorbent assay (ELISA) kits following the manufacturer's instructions. Measurements were performed using Mouse Lipocalin2 DuoSet (DY1857-05; R&D, Minneapolis, MN), Mouse IL6 DuoSet (DY406-05; R&D), and the IL22 Mouse ELISA Kit (88-7422-22; Invitrogen). LCN2 expression in both the intestine and liver were measured by Western blot analysis. The primary antibody, goat anti-LCN2 (1:500, AF1857; R&D), was incubated with a polyvinylidene difluoride membrane at 4°C overnight. The secondary antibody, anti-goat IgG Heavy and

light chains (H+L) (1:3000, HAF109; R&D), was incubated with a polyvinylidene difluoride membrane for 1 hour at room temperature.

Morphometric Analysis

The jejunum and ileum were fixed in 10% neutral buffered formalin for 24 hours. Fixed tissues were embedded in paraffin and cut into 5- μ m sections for H&E. The length of the villi were measured under light microscopy (EVOS FL Auto Imaging System, Life Technologies Corporation, Bothell, WA). At least 30 well-oriented intact villi were counted per mouse.

Immunohistofluorescence

The intestinal tissues were fixed in 4% paraformaldehyde for 24 hours. Fixed tissues then were embedded in paraffin and cut into 5- μ m sections for immunofluorescence staining. Slides were subjected to a deparaffinization and rehydration process. Antigen retrieval was performed in 10 mmol/L citric acid buffer pH 6.0 for 10 minutes at 100°C. Slides then were washed with PBS and blocked with 1% bovine serum albumin (9998S; Cell Signaling Technology, Danvers, MA) and 5% donkey serum (D9663; Sigma) at room temperature for 1 hour. The primary antibody, goat anti-lipocalin 2 (2 μ g/mL, AF1857; R&D), was applied to the tissue at 4°C overnight. The tissues were incubated with the secondary antibody, donkey anti-goat-555 (1:1000, A-21432; Invitrogen), at room temperature for 2 hours. The slides were rinsed with PBS, counterstained, and mounted in VECTASHIELD with 4',6-diamidino-2-phenylindole (H-1200; Vector Laboratories, Burlingame, CA). Imaging was performed with a confocal microscope (Nikon Eclipse Ti; Nikon Instruments Inc, Melville, NY).

Fecal DNA Isolation and 16S rRNA Gene Sequencing

Fecal DNA was isolated from the cecal contents with DNeasy PowerSoil kit (12888-100; Qiagen). V3-V4 regions of the 16S rRNA gene sequencing was performed on the Illumina (San Diego, CA) MiSeq platform at the Johns Hopkins Transcriptomics and Deep Sequencing Core. Subsequently, the intestinal microbiome was analyzed by Resphera Biosciences (Baltimore, MD).³⁷⁻³⁹ Raw paired-end read output by the MiSeq platform was merged into consensus fragments by FLASH and subsequently filtered for quality/length using Trimmomatic/QIIME. Passing sequences were trimmed of primers, evaluated for chimeras with UCLUST, and screened for mouse-associated contaminant using Bowtie2. Chloroplast/mitochondrial contaminants were detected and filtered using the Ribosomal Database Project classifier. High-quality 16S sequences were assigned to OTUs with a high-resolution taxonomic lineage using Resphera Insight. Contaminants were identified by searching for highly enriched species/OTUs in available negative control blank tubes (minimum 10-fold enrichment in blanks compared with nonblanks). Contaminant-filtered sequences were analyzed further by PICRUST to infer

functional content and aggregated at KEGG levels 1, 2, or 3. Taxonomic profiles then were subsampled to an even level of coverage before downstream statistical comparisons. α - and β -diversity analyses were performed using QIIME. PERMANOVA was applied for β -diversity comparative analysis. Differential abundance analysis was performed for all taxonomic groups (phylum through species/OTUs), α -diversity measures, and PICRUST functional categories. *P* values were adjusted using the false-discovery rate to account for multiple hypothesis testing.

Creation of Fecal Slurry From Cecal Contents and FMT

Five-week-old GF mice were divided randomly into 2 groups. Body weight was obtained before FMT. The 4% fecal slurries were created from the cecal contents of conventional WT SBR and LCN2^{-/-} SBR mice, respectively, and gavage-fed (100 μ L/mouse) to GF mice. Seven days after FMT, their body weight, intestinal permeability, and histology were evaluated.

Intestinal LPL Isolation and Cell Surface and Intracellular Staining for Flow Cytometry

The mesentery was removed from the harvested small intestine. The small intestine was opened longitudinally and cut into 5-mm pieces. After incubation with 0.1 mmol/L EDTA in Dulbecco's modified Eagle medium (21068-028; Gibco, Carlsbad, CA) with 10% fetal bovine serum (FBS) (35-010-CV; Corning, NY) for 1 hour at 37°C at 200 rpm, epithelial cells and intraepithelial lymphocytes were removed by passage through a 100- μ m cell strainer. The remaining lamina propria, muscle, and serosa layers were mechanically minced and incubated with Dulbecco's modified Eagle medium with 50 U/mL collagenase (LS004130; Worthington-Biochemical Corporation, Lakewood, NJ) for 45 minutes at 37°C at 200 rpm. A single-cell suspension was obtained by passing the cells through a 70- μ m cell strainer, and then subjecting the cells to a Percoll gradient (44% and 67%) (GE17-0891-01; Sigma) separation at room temperature for 20 minutes at 600 $\times g$. LPLs were collected from the interface between 44% and 67% Percoll solution and washed with PBS.

LPLs were stimulated in complete media (RPMI 1640 with 2 mmol/L L-glutamine, 10% FBS, 50 mmol/L β -mercaptoethanol (β -ME), and 100 U/mL penicillin-streptomycin) with cell stimulation cocktail plus protein transport inhibitors (00-4975-03; eBioscience, Carlsbad, CA), which were formulated with phorbol 12-myristate 13-acetate (80 nmol/L), ionomycin (1.34 μ mol/L), brefeldin A (10.6 μ mol/L), and monensin (2 μ mol/L) at 37°C for 5 hours. LPLs then were fixed and permeabilized (554714; BD, Franklin Lakes, NJ) at 4°C for 20 minutes and stained with an antibody cocktail, including peridinin-Chlorophyll-Protein (PerCP)-Cy5.5 rat anti-mouse CD4 (clone RM4-5, 1:200, 561115; BD), and allophycocyanin (APC) rat anti-mouse/human/monkey IL22 (IL22 JOP, 1:100, 17-7222-80; eBioscience) in 1 \times Perm/Wash buffer (554723; BD) at 4°C for 30 minutes. The cells were washed twice with 1 \times

Table 1. Primers

Gene	Forward primer	Reverse primer	Amplicon length, bp
<i>Lcn2</i>	AAGGAACGTTTCACCCGCTT	AATGCATTGGTCGGTGGGGA	84
<i>Tnf-α</i>	TTCCGAATTCACCTGGAGCCTCGAA	TGCACCTCAGGGAAGAATCTGGAA	144
<i>Il6</i>	CCAATTTCCAATGCTCTCCT	ACCACAGTGAGGAATGTCCA	182
<i>Il22</i>	CGACCAGAACATCCAGAAGAA	GAGACATAAACAGCAGGTCCA	110
<i>Reg3g</i>	GTACCCTGTCAAGAGCCTCA	GTACCCTGTCAAGAGCCTCA	184
<i>Reg3b</i>	GCTCAATAGCGCTGAGGCTT	AGAAAGCACGGTCTAAGGCA	200
<i>Hprt</i>	GCTGACCTGCTGGATTACATTAA	TGATCATTACAGTAGCTCTTCAGTCTGA	101
Sucrase-isomaltase	ATCCAGTTTCGAAGGAGAAGCACT	TTCGCTTGAATGCTGTGTGTTCCG	154
<i>Tgr5</i>	CAGCTGCCCAAAGGTGTCTA	CAAGTCCAGGTCAATGCTGC	110

Table 2. 16S rRNA Gene Target Group Primers

Target group	Forward primer	Reverse primer	Amplicon length, bp
Deltaproteobacteria	GCTAACGCATTAAGTRYCCCG	GCCATGCRGCACCTGTCT	189
Betaproteobacteria	AACGCGAAAAACCTTACCTACC	TGCCCTTTCGTAGCAACTAGTG	174
Epsilonproteobacteria	TAGGCTTGACATTGATAGAATC	CTTACGAAGGCAGTCTCCTTA	189
Bacteroidetes	GGARCATGTGGTTAATTCGATGAT	AGCTGACGACAACCATGCAG	127
Firmicutes	GGAGYATGTGGTTAATTCGAAGCA	AGCTGACGACAACCATGCAC	123
Universal 16S	AAACTCAAAGAATTGACGG	CTCACRRACGAGCTGAC	136

Perm/Wash buffer and suspended in fluorescence-activated cell sorter buffer (PBS with 0.5% bovine serum albumin, A8412; Sigma) before flow-cytometric analysis.

Naïve CD4⁺ T-Lymphocyte Isolation and Th22 Cell Differentiation

We isolated naïve CD4⁺ T cells as previously described by Bedoya et al⁴⁰ Briefly, splenic tissue was removed from 6-week-old C57BL/6J male mice and ground into a single-cell suspension under a sterile hood. Red blood cells were removed by using ammonium-chloride-potassium lysing buffer (118-156-101; Quality Biological, Gaithersburg, MD) at room temperature for 3 minutes. Naïve CD4⁺ T cells were isolated from total splenocyte by magnetic activated cell sorting based on positive selection using CD4 (L3T4) MicroBeads (130-117-043; Miltenyi Biotec, Bergisch-Gladbach, Germany) according to the manufacturer's instructions. The purity of naïve CD4⁺ T cells was more than 97%, as measured by flow cytometry.

For Th22 cell differentiation, CD4⁺ T cells were stimulated in complete media (RPMI 1640 with 2 mmol/L L-glutamine, 10% FBS, 50 mmol/L β -ME, and 100 U/mL penicillin-streptomycin) with plate-bound anti-CD3 ϵ (clone 145-2C11, 1 μ g/mL, 550275; BD) and soluble anti-CD28 (clone 37.51, 2 μ g/mL, 553295; BD) for 5 days under polarizing conditions for Th22 cells (20 ng/mL IL6, 10 ng/mL IL1 β , 10 ng/mL TNF- α)⁴¹ with and without rmlCN2 (1 μ g/mL, 1857-LC-050; R&D). Cell supernatant was collected for IL22 ELISA analysis (88-7422-22; Invitrogen) according to the manufacturer's instructions.

Rescue IL22 Therapy for SBR WT Mice

After a 75% SBR, WT mice were treated daily for 6 days via intraperitoneal injections with either 100 μ L PBS as control or 100 μ L PBS containing 4 μ g rmlL22 (210-22; PeproTECH) as treatment. On POD 7, intestinal tissue and cecal contents were collected after euthanasia. The relative abundance of Proteobacteria, Bacteroidetes, Firmicutes, Lactobacillus, and Enterobacteriaceae of the fecal microbiome and the *Reg3b* and *Reg3g* genes in the intestine were assessed by quantitative PCR.

RNA Extraction and Reverse Transcription

Total RNA from tissue was extracted according to the manufacturer's instructions (RNeasy Mini Kit, 74106; Qiagen). Genomic DNA was eliminated from RNA, and total RNA (0.5 μ g) was reverse-transcribed to complementary DNA with the QuantiTect Reverse Transcription Kit according to the manufacturer's protocol (205311; Qiagen, Germantown, MD).

Quantitative Real-Time PCR

Gene quantification was performed with the iTap Universal SYBR Green Supermix (172-5124; Bio-Rad, Hercules, CA) on a CFX96 Touch Real-time PCR system (Bio-Rad) according to the manufacturer's instructions and calculated with the 2^{- $\Delta\Delta$ CT} method. Thermal cycling was performed at 95°C for 5 minutes, followed by 40 cycles at 95°C for 15 seconds, 60°C for 10 seconds, and 72°C for 30 seconds. Primers for transcriptional levels of *Lcn2*, *Il6*, *sucrase-isomaltase*, *Tnf- α* , *Il22*, *Reg3b*, and *Reg3g* in intestine or liver

are listed in Table 1. Primers for fecal microbiome analysis in WT SBR mice that were treated with rmlL22 mRNA are listed in Table 2.

Statistical Analysis

Statistical analysis was performed using Prism 5.0 (GraphPad Software, San Diego, CA). The Student *t* test was used to analyze statistical differences between 2 groups. Analysis of variance with a Bonferroni post-test correction was used to calculate statistical differences between 3 or 4 groups. 16S rRNA microbiome analysis was described earlier in the *Fecal DNA Isolation and 16S rRNA Gene Sequencing* section. Values of *P* < .05 were considered significant.

References

- Duggan CP, Jaksic T. Pediatric Intestinal Failure. *N Engl J Med* 2017;377:666–675.
- Squires RH, Duggan C, Teitelbaum DH, Wales PW, Balint J, Vernick R, Rhee S, Sudan D, Mercer D, Martinez JA, Carter BA, Soden J, Horslen S, Rudolph JA, Kocoshis S, Superina R, Lawlor S, Haller T, Kurs-Lasky M, Belle SH. Pediatric Intestinal Failure Consortium. Natural history of pediatric intestinal failure: initial report from the Pediatric Intestinal Failure Consortium. *J Pediatr* 2012;161:723–728.e2.
- Fullerton BS, Hong CR, Jaksic T. Long-term outcomes of pediatric intestinal failure. *Sem Ped Surg* 2017;26:328–335.
- Engstrand LH, Wefer H, Nystrom N, Finkel Y, Engstrand L. Intestinal dysbiosis in children with short bowel syndrome is associated with impaired outcome. *Microbiome* 2015;3:18.
- Davidovics ZH, Carter BA, Luna RA, Hollister EB, Shulman RJ, Versalovic J. The fecal microbiome in pediatric patients with short bowel syndrome. *JPEN J Parenter Enteral Nutr* 2016;40:1106–1113.
- Piper HG, Fan D, Coughlin LA, Ho EX, McDaniel MM, Channabasappa N, Kim J, Kim M, Zhan X, Xie Y, Koh AY. Severe gut microbiota dysbiosis is associated with poor growth in patients with short bowel syndrome. *JPEN J Parenter Enteral Nutr* 2017;41:1202–1212.
- Sears CL. Molecular physiology and pathophysiology of tight junctions V. Assault of the tight junction by enteric pathogens. *Am J Physiol Gastrointest Liver Physiol* 2000;279:G1129–G1134.
- Kelly DA. Preventing parenteral nutrition liver disease. *Early Hum Dev* 2010;86:683–687.
- Deitch EA, Sittig K, Li M, Berg R, Specian RD. Obstructive jaundice promotes bacterial translocation from the gut. *Am J Surg* 1990;159:79–84.
- Alaish SM, Smith AD, Timmons J, Greenspon J, Eyvazzadeh D, Murphy E, Shea-Donahue T, Cirimotich S, Mongodin E, Zhao A, Fasano A, Nataro JP, Cross A. Gut microbiota, tight junction protein expression, intestinal resistance, bacterial translocation and mortality following cholestasis depend on the genetic background of the host. *Gut Microbes* 2013;4:292–305.
- Marchix J, Goddard G, Helmrath MA. Host-gut microbiota crosstalk in intestinal adaptation. *Cell Mol Gastroenterol Hepatol* 2018;6:149–162.
- Nasioudis D, Witkin SS. Neutrophil gelatinase-associated lipocalin and innate immune responses to bacterial infections. *Med Microbiol Immunol* 2015;204:471–479.
- Goetz DH, Holmes MA, Borregaard N, Bluhm ME, Raymond KN, Strong RK. The neutrophil lipocalin NGAL is a bacteriostatic agent that interferes with siderophore-mediated iron acquisition. *Mol Cell* 2002;10:1033–1043.
- Flo TH, Smith KD, Sato S, Rodriguez DJ, Holmes MA, Strong RK, Akira S, Aderem A. Lipocalin 2 mediates an innate immune response to bacterial infection by sequestering iron. *Nature* 2004;432:917–921.
- Berger T, Togawa A, Duncan GS, Elia AJ, You-Ten A, Wakeham A, Fong HE, Cheung CC, Mak TW. Lipocalin 2-deficient mice exhibit increased sensitivity to *Escherichia coli* injection but not to ischemia-reperfusion injury. *Proc Natl Acad Sci U S A* 2006;103:1834–1839.
- Alaish SM, Timmons J, Smith A, Buzza MS, Murphy E, Zhao A, Sun Y, Turner DJ, Shea-Donahue T, Antalis TM, Cross A, Dorsey SG. Candidate genes for limiting cholestatic intestinal injury identified by gene expression profiling. *Physiol Rep* 2013;1.
- Wildhaber BEH, Yang H, Coran AG, Teitelbaum DH. Gene alteration of intestinal intraepithelial lymphocytes in response to massive small bowel resection. *Ped Surg Int* 2003;19:310–315.
- Helmrath MA, VanderKolk WE, Can G, Erwin CR, Warner BW. Intestinal adaptation following massive small bowel resection in the mouse. *J Am Coll Surg* 1996;183:441–449.
- Zheng Y, Valdez PA, Danilenko DM, Hu Y, Sa SM, Gong Q, Abbas AR, Modrusan Z, Ghilardi N, de Sauvage FJ, Ouyang W. Interleukin-22 mediates early host defense against attaching and effacing bacterial pathogens. *Nat Med* 2008;3:282–289.
- Ye D, Yang K, Zang S, Lin Z, Chau HT, Wang Y, Zhang J, Shi J, Xu A, Lin S, Wang Y. Lipocalin-2 mediates non-alcoholic steatohepatitis by promoting neutrophil-macrophage crosstalk via the induction of CXCR2. *J Hepatol* 2016;65:988–997.
- Wu G, Li H, Fang Q, Jiang S, Zhang L, Zhang J, Hou X, Lu J, Bao Y, Xu A, Jia W. Elevated circulating lipocalin-2 levels independently predict incident cardiovascular events in men in a population-based cohort. *Arterioscler Thromb Vasc Biol* 2014;34:2457–2464.
- Tarin C, Fernandez-Garcia CE, Burillo E, Pastor-Vargas C, Llamas-Granda P, Castejon B, Ramos-Mozo P, Torres-Fonseca MM, Berger T, Mak TW, Egidio J, Blanco-Colio LM, Martin-Ventura JL. Lipocalin-2 deficiency or blockade protects against aortic abdominal aneurysm development in mice. *Cardiovasc Res* 2016;111:262–273.
- Law IK, Xu A, Lam KS, Berger T, Mak TW, Vanhoutte PM, Liu JT, Sweeney G, Zhou M, Yang B, Wang Y. Lipocalin-2 deficiency attenuates insulin

- resistance associated with aging and obesity. *Diabetes* 2010;59:872–882.
24. Oikonomou KA, Kapsoritakis AN, Theodoridou C, Karangelis D, Germenis A, Stefanidis I, Potamianos SP. Neutrophil gelatinase-associated lipocalin (NGAL) in inflammatory bowel disease: association with pathophysiology of inflammation, established markers, and disease activity. *J Gastroenterol* 2012;47:519–530.
 25. Staley C, Khoruts A, Sadowsky MJ. Contemporary applications of fecal microbiota transplantation to treat intestinal diseases in humans. *Arch Med Res* 2017;48:766–773.
 26. Al-Asmakh M, Zadjilil F. Use of germ-free animal models in microbiota-related research. *J Microbiol Biotechnol* 2015;25:1583–1588.
 27. Sanjabi S, Zenewicz LA, Kamamaka M, Flavell RA. Anti- and pro-inflammatory roles of TGF- β , IL-10, and IL-22 in immunity and autoimmunity. *Curr Opin Pharmacol* 2009;9:447–453.
 28. Alabbas SY, Begun J, Florin TH, Oancea I. The role of IL-22 in the resolution of sterile and nonsterile inflammation. *Clin Transl Immunology* 2018;7:e1017.
 29. Shabgah AG, Navashenaq JG, Shabgah OG, Mohammadi H, Sahebkar A. Interleukin-22 in human inflammatory diseases and viral infections. *Autoimmun Rev* 2017;16:1209–1218.
 30. Eyerich K, Dimartino V, Cavani A. IL-17 and IL-22 in immunity: driving protection and pathology. *Eur J Immunol* 2017;47:607–614.
 31. Zenewicz LA, Yancopoulos GD, Valenzuela DM, Murphy AJ, Karow M, Flavell RA. Interleukin-23 but not interleukin-17 provides protection to hepatocytes during acute liver inflammation. *Immunity* 2007;27:647–659.
 32. Zenewicz LA, Yancopoulos GD, Valenzuela DM, Murphy AJ, Stevens S, Flavell RA. Innate and adaptive interleukin-22 protects mice from inflammatory bowel disease. *Immunity* 2008;29:947–957.
 33. Sugimoto K, Ogawa A, Mizoguchi E, Shimomura Y, Andoh A, Bhan AK, Blumberg RS, Xavier RJ, Mizoguchi A. IL-22 ameliorates intestinal inflammation in a mouse model of ulcerative colitis. *J Clin Invest* 2008;118:534–544.
 34. Zheng Y, Danilenko DM, Valdez P, Kasman I, Eastham-Anderson J, Wu J, Ouyang W. Interleukin-22, a T(H) 17 cytokine, mediates IL-23-induced dermal inflammation and acanthosis. *Nature* 2007;445:648–651.
 35. Hammer AM, Morris NL, Cannon AR, Khan OM, Gagnon RC, Movtchan NV, van Langeveld I, Li X, Gao B, Choudhry MA. Interleukin-22 prevents microbial dysbiosis and promotes intestinal barrier regeneration following acute injury. *Shock* 2017;48:657–665.
 36. Raetz M, Hwang S, Wilhelm CI, Kirkland D, Benson A, Sturge CR, Mirpuri J, Vaishnav S, Hou B, Defranco AL, Gilpin CJ, Hooper LV, Yarovinsky F. Parasite-induced Th1 cells and intestinal dysbiosis cooperate in IFN- γ -dependent elimination of Paneth cells. *Nat Immunol* 2013;14:136–144.
 37. Drewes JL, White JR, Dejea CM, Fathi P, Iyadoral T, Vadivelu J, Roslani AC, Wick EC, Mongodin EF, Loke MF, Thulasi K, Gan HM, Goh KL, Chong HY, Kumar S, Wanyiri JW, Sears CL. High-resolution bacterial 16S rRNA gene profile meta-analysis and biofilm status reveal common colorectal cancer consortia. *NPJ Biofilms Microbiomes* 2017;3:34.
 38. Daquigan N, Seekatz AM, Greathouse KL, Young VB, White JR. High-resolution profiling of the gut microbiome reveals the extent of *Clostridium difficile* burden. *NPJ Biofilms Microbiomes* 2017;3:35.
 39. Grim CJ, Daquigan N, Lusk Pfefer TS, Ottesen AR, White JR, Jarvis KG. High-resolution microbiome profiling for detection and tracking of *Salmonella enterica*. *Front Microbiol* 2017;8:1587.
 40. Bedoya S, Wilson TD, Collins EL, Lau K, Larkin J 3rd. Isolation and Th17 differentiation of naïve CD4 T lymphocytes. *J Vis Exp* 2013;79:e50765.
 41. Plank MW, Kaiko GE, Maltby S, Weaver J, Tay HL, Shen W, Wilson MS, Durum SK, Foster PS. Th22 cells form a distinct Th lineage from Th17 cells in vitro with unique transcriptional properties and Tbet-dependent Th1 plasticity. *J Immunol* 2017;198:2182–2190.

Received January 31, 2020. Accepted April 10, 2020.

Correspondence

Address correspondence to: Samuel M. Alaish, MD, Department of Surgery, Johns Hopkins University School of Medicine, 1800 Orleans Street, Suite 7337, Baltimore, Maryland 21287. e-mail: salaish1@jhmi.edu; fax: (443) 769-1287.

CRedit Authorship Contributions

Ailan Zhang, MD, PhD (Conceptualization: Lead; Data curation: Lead; Formal analysis: Lead; Methodology: Lead; Project administration: Lead; Software: Lead; Validation: Lead; Writing – original draft: Lead; Writing – review & editing: Lead); Chhinder P. Sodhi, PhD (Conceptualization: Lead; Formal analysis: Equal; Methodology: Lead; Supervision: Lead); Menghan Wang, MS (Formal analysis: Supporting; Methodology: Equal); Darla R. Shores, MD, PhD (Conceptualization: Equal; Data curation: Equal; Project administration: Equal); William B. Fulton, MS (Methodology: Equal; Software: Equal); Thomas Prindle, BS (Methodology: Equal); Serena D. Brosten, BA (Data curation: Equal; Methodology: Equal); Elizabeth M. O’Hare, BS (Data curation: Supporting; Methodology: Equal); Alexander R. Lau, BS (Formal analysis: Supporting; Methodology: Equal); Hua Ding, MD (Formal analysis: Equal; Methodology: Supporting); Hongpeng Jia, MD (Data curation: Equal; Formal analysis: Equal; Methodology: Equal); Peng Lu, PhD (Data curation: Equal; Formal analysis: Equal; Methodology: Lead); James R. White, PhD (Formal analysis: Equal; Methodology: Equal); Justin Hui, BS (Data curation: Supporting; Formal analysis: Supporting); Cynthia L. Sears, MD (Conceptualization: Equal; Formal analysis: Equal); David J. Hackam, MD, PhD (Conceptualization: Lead; Formal analysis: Lead); Samuel M. Alaish, MD (Conceptualization: Lead; Data curation: Lead; Formal analysis: Lead; Funding acquisition: Lead; Investigation: Lead; Methodology: Equal; Project administration: Lead; Resources: Lead; Validation: Lead; Writing – original draft: Lead; Writing – review & editing: Lead).

Conflicts of interest

The authors disclose no conflicts.

Funding

This work was supported by the Garrett Foundation and the Hartwell Foundation (Grant # 126558).